J. Biochem. 127, 945–953 (2000)

Backbone Dynamics of the c-Myb DNA-Binding Domain Complexed with a Specific DNA[1]

Motoko Sasaki,[*,†] Kazuhiro Ogata,[†,‡] Hideki Hatanaka,[§] and Yoshifumi Nishimura[*,‖,2]

[*]Graduate School of Integrated Science, Yokohama City University, 22-2 Seto, Kanazawa-ku, Yokohama 236-0027; [†]Kanagawa Academy of Science and Technology, 3-9 Fukuura, Kanazawa-ku, Yokohama 236-0004; [‡]Department of Structural Biology, Yokohama City University School of Medicine, 3-9 Fukuura, Kanazawa-ku, Yokohama 236-0004; [§]Department of Molecular Physiology, The Tokyo Metropolitan Institute of Medical Science, 3-18-22 Honkomagome, Bunkyo-ku, Tokyo; and [‖]Genomic Sciences Center (GSC), RIKEN (The Institute of Physical and Chemical Research), 2-1 Hirosawa, Wako, Saitama 351-0198

Received February 1, 2000; accepted February 17, 2000

The DNA-binding domain of c-Myb consists of three imperfect tandem repeats, R1, R2, and R3. Each repeat contains three helices. The minimal DNA-binding domain is an R2R3 fragment. Here, we have examined the backbone dynamics of R2R3 in its DNA-bound form by NMR. Upon binding to DNA, the N- and C-termini, and the linker between R2 and R3 become less flexible. In the free form the third helix of R2 exhibits slow conformational exchange fluctuations owing to a cavity in the hydrophobic core of R2. Upon binding to DNA, the conformational exchange contributions in R2 are reduced but remain significant in NMR relaxation measurements. Upon binding to DNA, the third helix of R3 comes to exhibit significant chemical exchange contributions. These findings suggest that the orientations of the third helices of both R2 and R3 as to DNA are being chemically exchanged. In the DNA-bound form both R2 and R3 exhibit similar dynamical characters, except for amino acids Trp 95, Thr 96, and Val 103 of R2, which are located around the cavity of the unbound form. Upon binding to DNA, since Trp 95 moves into the cavity to fill it up, the local conformational exchange contributions seem to be still observable around the filled cavity.

Key words: c-Myb, complex with DNA, DNA-binding domain, dynamics, NMR.

The c-*myb* protooncogene is the cellular homologue of the viral *myb* oncogene, which was first identified in two chicken retroviruses, avian myeloblastosis virus (AMV) and E26 (*1–4*). The c-*myb* gene product, c-Myb protein, binds specifically to DNA containing the consensus sequence, PyAAC(G/T)G (*5–8*) and acts as a transcriptional activator. Using c-*myb* gene knock-out mice, it was found that the c-*myb* gene is essential for fetal hepatic hematopoiesis in embryonic development (*9*). The mouse c-Myb, consisting of 636 amino acids, is composed of three functional domains, *i.e.* DNA binding, transcription activation, and negative transcription regulation domains, from the N-terminus (*10*). The DNA binding domain consists of three imperfect tandem repeats of 51 to 52 amino acids, designated as R1, R2, and R3 from the N-terminus (*10–12*). The R2R3 fragment is essential for the specific DNA recognition by c-Myb as the minimal DNA-binding domain (*9, 13*).

The solution structures of isolated R1, R2, and R3 fragments as well as R1R2R3 were determined by NMR (*14, 15*). Each repeat contains three helices maintained by a hydrophobic core including three conserved tryptophan residues. The second and third helices in each repeat form a helix-turn-helix (HTH) variant motif, containing a turn of one amino acid residue longer than that in the classical HTH motif. Although the tertiary structures of three repeats are very similar to each other, R2 is thermally less stable than R1 and R3. The T_m of R2 is 43°C, whereas the T_ms of R1 and R3 are 61 and 57°C, respectively (*16*). This thermal instability of R2 is due to the presence of a cavity in its hydrophobic core. A cavity filled mutant, V103L, in which the valine residue at 103 is replaced by a leucine residue, becomes thermally stable with a T_m of 62°C. NMR relaxation experiments on R2R3 in the free form have revealed that thermally unstable R2 exhibits great conformational fluctuations on the micro- to milli-second time scale, especially in the third helical region (*17*), while R3 shows no significant conformational fluctuations on the micro- to milli-second time scale. On the other hand, in the thermally stabilized mutant (V103L) of R2R3 the slow conformational fluctuations are greatly suppressed (*17*). Therefore a possible correlation between the thermal stability and slow conformational fluctuations has been obtained. The thermally stabilized mutant exhibits less DNA-binding

[1] This work was supported by Grants-in-Aid for Scientific Research (06276103, 06276104, 11358012, and 11154221 to YN) from the Ministry of Education, Science, Sports and Culture of Japan, and partly by an HFSP program (YN) and The Mitsubishi Foundation (YN).

[2] To whom correspondence should be addressed at: Graduate School of Integrated Science, Yokohama City University, 22-2 Seto, Kanazawa-ku, Yokohama 236-0027. Tel: +81-45-787-2188, Fax: +81-45-787-2370, e-mail: nisimura@yokohama-cu.ac.jp

Abbreviations: CPMG, Carr-Purcell-Meiboom-Gill; HMQC, heteronuclear multiple quantum coherence; HSQC, heteronuclear single quantum coherence; NOE, nuclear Overhauser effect; NOESY, nuclear Overhauser enhancement spectroscopy; SD, standard deviation.

ability compared to the wild type. The structure of R2R3 complexed with a specific DNA has also been established (*18*). In the specific DNA complex of R2R3 each repeat contains a three helix-containing structure similar to the unbound form. The third helices of both R2 and R3 are closely packed in the major groove of DNA, recognizing a specific consensus sequence cooperatively. In the complex the tryptophan residue at position 95 moves into the cavity of R2. So the cavity of R2 found in the unbound form is reserved for the conformational change induced by the specific DNA-binding (*17*).

Here, we have examined the backbone dynamics of R2R3 complexed with a specific DNA and compared it with that of the unbound form of R2R3. The chemical exchange contributions in the third helical region of R2 are suppressed upon binding to DNA, but remain significant. On the other hand, upon binding to DNA the third helical region of R3 comes to exhibit great chemical exchange contributions. These findings suggest that the orientations of the third helices of both R2 and R3 as to DNA are being chemically exchanged.

MATERIALS AND METHODS

Sample Preparation—The DNA binding domain of mouse c-Myb, the R2R3 fragment consisting of 90–193 amino acids (Fig. 1a), was expressed in *Escherichia coli* BL21(DE3) using a T7 expression system. The construct used includes an N-terminal methionine. The uniformly ^{15}N labeled sample was overexpressed in M9 minimal medium containing $^{15}NH_4Cl$ (1.5 g/liter) and purified as described previously (*18*).

Here, we have examined a 13 bp DNA complex of R2R3 with the sequence of CCTAACTGACACA (Fig. 1b), instead of a 16 bp DNA complex which was used for the structure determination (*18*). On the basis of the determined structure of the 16 bp DNA complex, the 13 bp DNA was found to be sufficient for the complex formation of R2R3. The K_d value of R2R3 for the 13 bp DNA was found to be 4.6×10^{-9} M, which is similar to the value for the 16 bp DNA, 3.8×10^{-9} M. In addition, the shape of the 13 bp DNA complex is apparently much more globular than that of the 16 bp DNA complex. If the *z* axis is defined along the DNA axis, the 13 bp DNA complex is a nearly cubic box of 48 Å × 40 Å × 54 Å along the *x*, *y*, and *z* axes, respectively.

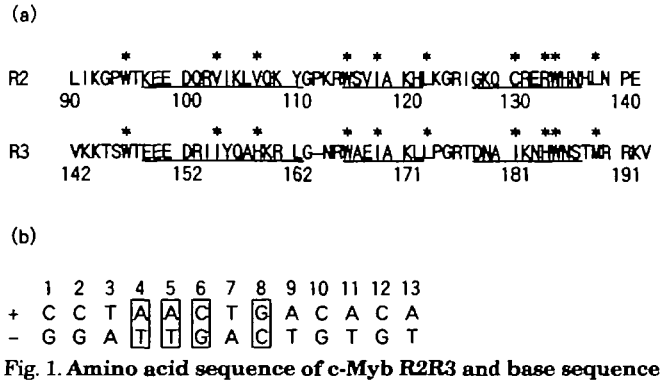

Fig. 1. **Amino acid sequence of c-Myb R2R3 and base sequence of the 13 bp DNA duplex.** (a) Amino acid sequence of c-Myb R2R3. The residues involved in the hydrophobic core are denoted by asterisks. The bars below the residues indicate helical regions. (b) Base sequence of the 13 bp DNA duplex. The bases specifically recognized by c-Myb are boxed.

Complementary DNA fragments, 5′-CCTAACTGACACA-3′ and 5′-TGTGTCAGTTAGG-3′, purchased from BEX (Tokyo) were mixed in an equimolar ratio in 10 mM potassium phosphate buffer (pH 7.0), heated to 95°C and then annealed by cooling slowly to room temperature. Using a Centriprep (Amicon, USA), the duplex DNA solution is changed to a salt-free solution adjusted to pH 6.8, as measured with a PHM93 (Radiometer, Copenhagen), and is then concentrated to a 20 mM DNA solution. Aliquots of the concentrated double-strand DNA solution were added to the R2R3 solution (pH 6.8, 20 mM d_{10}-DTT, and 1 mM NaN_3) to get a final 1.2:1.0 ratio of DNA to protein, and then the pH was readjusted to pH 6.8. The 2.5 mM R2R3-DNA complex in 90% H_2O and 10% D_2O (pH 6.8) containing 20 mM d_{10}-DTT and 1 mM NaN_3 was used for NMR measurements.

NMR Spectroscopy—All NMR data were collected with a Bruker AMX 500 spectrometer at a temperature of 310 K. Heteronuclear single-quantum coherence (HSQC) (*19*) and 3D NOESY-HMQC (*20*, *21*) spectra with a mixing time of 100 ms were measured by a TPPI method. ^{15}N spin-lattice relaxation time, T_1, ^{15}N spin-spin relaxation time, T_2, ^{15}N spin-lattice relaxation time in the rotating frame, $T_{1\rho}$, and ^1H-^{15}N steady-state NOE experiments were performed as reported previously (*22–25*). Water suppression was achieved by spin-lock purge pulse for T_1, T_2, and $T_{1\rho}$ measurements or by weak presaturation of 100 ms duration besides the purge pulse for ^1H-^{15}N NOEs measurements. The spectral widths were 7,024 and 1,408 Hz for the ^1H and ^{15}N directions, respectively. The carrier was placed on the water resonance. The 2D heteronuclear spectra that were used for analysis of the relaxation parameters contained 256 f1 × 2048 f2 data points. The raw data were subsequently zero-filled in the f1 dimension. GARP-1 broad-band decoupling of the ^{15}N nucleus was used in the ^1H acquisition period. 256 transients per f1 increment were recorded for the T_1, T_2, and $T_{1\rho}$ measurements, and 412 transients were recorded for ^1H-^{15}N NOE measurements. For T_1, T_2, and $T_{1\rho}$ experiments, a recycle time of 2 s was used between acquisitions to ensure sufficient recovery of the ^1H magnetization. The T_1 measurements were performed using the inversion recovery method. Data were collected with delays of 10.04, 60.24, 110.44, 160.63, 261.03, 361.43, 512.02, 712.81, 963.80, and 1214.79 ms. The T_2 measurements were performed with the following transverse relaxation periods: 9.64, 19.27, 28.90, 38.53, 48.17, 57.80, 67.44, 77.07, and 86.70 ms. A 900 μs delay between successive pulses in the Carr-Purcell-Meiboom-Gill (CPMG) sequence was used during the relaxation period. The $T_{1\rho}$ measurements were performed using the CW spin-lock ^{15}N pulse applied with a field strength of 2.1 kHz during the following relaxation delays. Data were collected with the relaxation delays of 9.64, 19.27, 28.90, 38.53, 48.17, 57.80, 67.44, 77.07, and 86.70 ms. ^1H-^{15}N NOE spectra were recorded with and without presaturation of amide protons, *i.e.* NOE(+) and NOE(−) experiments. Two sets of experiments were carried out in order to estimate the uncertainty of the data. In the NOE(−) experiment, a relaxation delay of 5 s was employed between transients, while in the NOE(+) experiment a 2 s recycle delay was employed, followed by proton presaturation for 3 s prior to the first

^{15}N pulse. NMR spectra were processed using UXNMR and X-win NMR (Bruker Instruments).

Estimation of T_1, T_2, and $T_{1\rho}$, and Steady-State NOE—Cross-peaks of the spectra were integrated along their peaks sliced through the ^1H or ^{15}N dimension corresponding to the cross peak maxima. T_1, T_2, and $T_{1\rho}$ values were obtained from two parameter non-linear least square fits to the integrated values of cross-peaks *versus* relaxation delays in the T_1, T_2, and $T_{1\rho}$ experiments using the Levenberg-Marquart algorithm (*26*), *i.e.* $I(t) = I_0 \exp(-t/T_{1,2,1\rho})$, where $I(t)$ is the integrated value of a cross peak after a delay of time t and I_0 is the initial value. The uncertainties of the T_1, T_2, and $T_{1\rho}$ values were estimated from the root-mean-square noise in a signal-free region in the corresponding spectrum, instead of through repetitive experiments. The ^1H-^{15}N steady-state NOE values were determined as the ratio of the integrated values of cross peaks in NOE(+) and NOE(−) experiments, *i.e.* NOE = $I_{NOE(+)}/I_{NOE(-)}$. The uncertainties of the ^1H-^{15}N NOE values were estimated at 0.1 NOE units, considering the effects of weak water presaturation, except when the errors obtained from root-mean-square deviations of the pairwise spectra exceeded the limit of 0.1 NOE units.

Model-Free Analysis—The overall correlation time (τ_R) was calculated from a simultaneous fit of the $T_1/T_{1\rho}$ values that lie within 1 SD of the mean value and NOEs ≥ 0.7 for amino acid residues W95–W185. The relaxation parameters were analyzed using the model-free approach of Lipari and Szabo (*27*, *28*) with a modification by Clore *et al.* (*29*, *30*), as follows:

$$1/T_1 = d^2[J(\omega_H-\omega_N) + 3J(\omega_N) + 6J(\omega_H + \omega_N)] + c^2J(\omega_N)$$

$$1/T_2 = 0.5d^2[4J(0) + J(\omega_H - \omega_N) + 3J(\omega_N) + 6J(\omega_H) + 6J(\omega_H + \omega_N)] + c^2[4J(0) + 3J(\omega_N)]/6$$

$$NOE = 1 + T_1(\gamma_H/\gamma_N)\, d^2[6J(\omega_H + \omega_N) - J(\omega_H - \omega_N)]$$

where ω_H and ω_N are the Larmor frequencies for ^1H and ^{15}N, γ_H and γ_N are the ^1H and ^{15}N magnetogyric ratios, and c^2 and d^2 are the products of physical constants relevant to CSA and dipolar relaxation mechanisms, respectively. The dipolar constant $d^2 = (1/40)\, \gamma_H^2\, \gamma_N^2\, h^2\, r_{HN}^{-6}$, and the CSA constant $c^2 = (2/15)\, \omega_N^2\, (\sigma_\parallel - \sigma_\perp)^2$, where h is Planck's constant, r_{HN} =1.02 Å is the average length of ^{15}N-^1H bond, and $\sigma_\parallel$ and $\sigma_\perp$ are the parallel and perpendicular components of the amide NH ^{15}N chemical shift tensor ($\sigma_\parallel - \sigma_\perp$ = −160 ppm). The spectral density function, $J(\omega)$, defines the frequency spectrum of autocorrelation functions describing the motion of the N-H bond. Exchange contributions to $1/T_2$, due to motions on the micro- to milli-second time scale, were treated by adding a third term, Rex, to the equation of $1/T_2$. The spectral density function is modelled as follows.

model 1: $J(\omega) = S^2\tau_R/(1 + \omega^2\tau_R^2)$

model 2: $J(\omega) = S^2\tau_R/(1 + \omega^2\tau_R^2) + (1 - S^2)\tau/(1 + \omega^2\tau^2)$

model 3: $J(\omega) = S_f^2S_s^2\tau_R/(1 + \omega^2\tau_R^2) + S_f^2(1 - S_s^2)\tau_s'/(1 + \omega^2\tau_s'^2)$

model 4: model 1 and $1/T_2 = 1/T_2 + Rex$

model 5: model 2 and $1/T_2 = 1/T_2 + Rex$

where S is the generalized order parameter (which depends on the amplitudes of pico- to nano-second time scale motions), τ_R is the overall rotational correlation time, τ is an effective correlation time resulting from internal motions characterized by a single internal correlation time, τ_e($1/\tau = 1/\tau_e + 1/\tau_R$), S_f and S_s are order parameters corresponding to fast and slow internal pico- to nano-second motions with time scales differing by at least an order magnitude, respectively (note: $S^2 = S_f^2S_s^2$), and τ_s' is an effective correlation time resulting from the slow correlation time, τ_s ($1/\tau_s' = 1/\tau_s + 1/\tau_R$).

The form of the spectrum density function in each residue was selected using the strategy of Constantine *et al.* (*31*), as follows.

NOE ≥ 0.7 and $T_1/T_2 \geq \langle T_1/T_2\rangle$ − SD → model 4

NOE ≥ 0.7 and $T_1/T_2 \leq \langle T_1/T_2\rangle$ + SD → model 1

NOE ≤ 0.7 and $T_1/T_2 \leq \langle T_1/T_2\rangle$ + SD → model 2

NOE ≤ 0.7 and $T_1/T_2 \geq \langle T_1/T_2\rangle$ − SD → model 5

where $\langle T_1/T_2\rangle$ is the average of the T_1/T_2 values. If the two models could be applied to one residue, the model without Rex was selected except when the model with Rex had an explicitly lower χ^2 value, where $\chi^2 = [(T_{1exp} - T_{1calc})/\sigma_{T1}]^2 + [(T_{2exp} - T_{2calc})/\sigma_{T2}]^2 + [(NOE_{exp} - NOE_{calc})/\sigma_{NOE}]^2$: 'exp' and 'calc' refer to the experimental and calculated relaxation parameters, respectively, and σ_x is the uncertainty in relaxation parameter x. Then NOE values were calculated based on derived parameters, and differences between calculated and experimental NOE values were determined.

If $(NOE_{exp} - NOE_{calc}) > NOE_{error}$

$T_1/T_2 \geq \langle T_1/T_2\rangle$ − SD → model 5

$T_1/T_2 \leq \langle T_1/T_2\rangle$ + SD → model 3

If the two models could be applied to one residue, the model having the lower χ^2 value was selected. The data fitting was performed by a non-linear least square method for two parameters using the Levenberg-Marquart algorithm. The uncertainties in the calculated values were estimated from the covariance matrix (*26*).

RESULTS

^{15}N Relaxation Data—Figure 2 shows the ^1H-^{15}N HSQC spectrum of the 13 bp DNA complex of ^{15}N-labeled R2R3. Based on the earlier assignments of the 16 bp DNA complex (*18*), the assignments of the 13 bp DNA complex have been completed by 3D NOESY-HMQC with a 100 ms mixing time. The signals of amide nitrogens and amide protons of R2R3 complexed with the 13 bp DNA were found at similar chemical shift positions to in the case of the 16 bp DNA complex within ±0.05 ppm for ^1H and ±0.1 ppm for ^{15}N signals. The 99 cross peaks, of which 48 are from R2 and 51 from R3, were assigned in the ^1H-^{15}N HSQC spectrum of the 13 bp DNA complex, as shown in Fig. 2. The cross peak of Asn 136 was not identified probably due to a line broadening effect caused by conformational exchange contributions. Pro 94, Pro 112, Pro 140, and Pro 174 have no cross peak. The relaxation data for the 27 cross peaks (19 from R2 and 8 from R3) out of the 99 cross peaks could not be well measured due to severe signal overlaps or line broadening effects caused by chemical exchange contributions. In particular, significant line broadening effects were observed for the signals from R2, for example Leu 106 in the first helix, Trp 115, Val 117, and Ile 118 in the second helix, and Cys 130, Arg 131, Glu 132, Arg 133, and His 135 in the third helix.

Figure 3a shows the T_1 values for each residue of R2R3 in its DNA-bound and unbound forms. The T_1 value for each residue of the DNA-bound form is always larger than that for the corresponding residue of the DNA-free form because of the larger molecular weight of the complex than that of the free form (*32–34*). The averages of the T_1 values

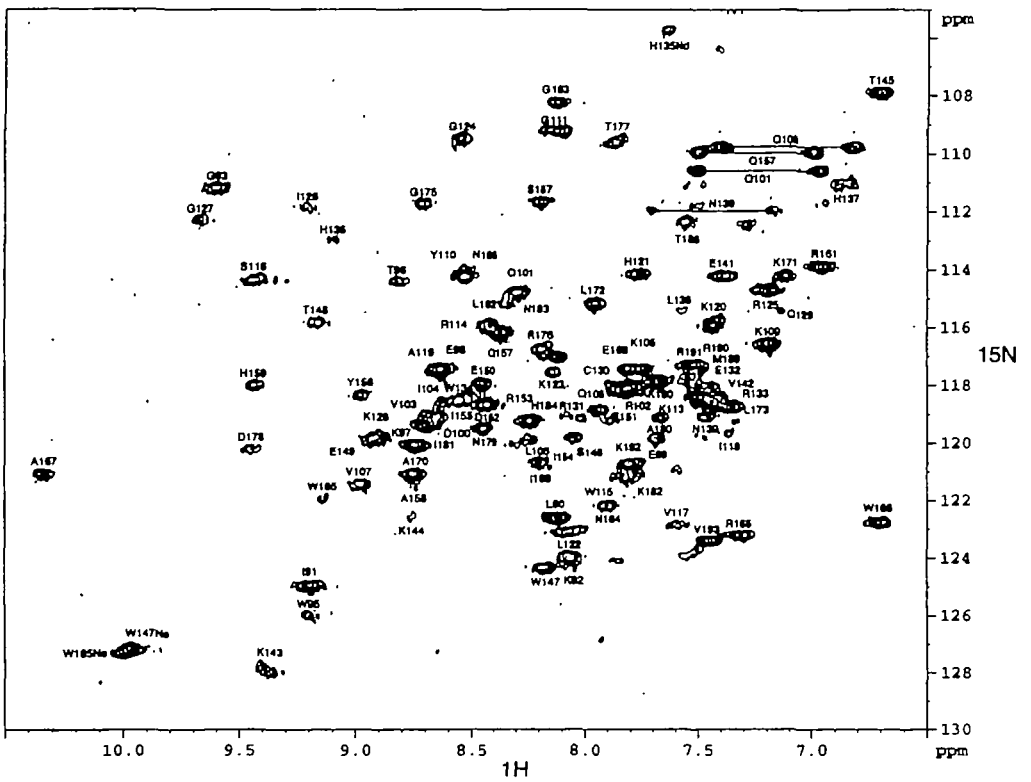

Fig. 2. **^{1}H-^{15}N HSQC spectrum of the R2R3-DNA complex.** The temperature during data acquisition was set at 310 K. The sample contained the 2.5 mM R2R3-DNA complex in a salt-free solution (pH 6.8) composed of 20 mM d_{10}-DTT and 1 mM NaN_3 in 90% H_2O, 10% D_2O.

for the three helical regions of the R2 and R3 moieties are 606 ± 50 and 585 ± 37 ms in the free form, and 802 ± 63 and 813 ± 74 ms in the complex, respectively. Figure 3b shows the T_2 values for each residue of R2R3 in its DNA-bound and unbound forms. The T_2 value for each residue of the DNA-bound form except amino acids of the third helical region of R2 is always smaller than that for the corresponding residue of the free form because of the larger molecular weight of the complex than the free form (*32*). The T_2 values of R2, especially in the third helical region in the free form, are small due to the slow conformational fluctuations caused by the presence of the cavity in the R2 hydrophobic core (*17*). The averages of the T_2 values for the R2 and R3 helical regions are 72.0 ± 13.7 and 89.2 ± 8.5 ms in the free form, and 57.1 ± 5.4 and 58.5 ± 7.3 ms in the DNA-bound form, respectively. Figure 3c shows the $T_{1\rho}$ values. The $T_{1\rho}$ value for each residue of the complex is smaller than that for the corresponding residue of the free form (*33*) because of the larger molecular weight of the complex. The averages of the $T_{1\rho}$ values for the R2 and R3 helical regions are 80.7 ± 7.9 and 89.1 ± 6.8 ms in the free form, and 68.9 ± 6.6 and 65.6 ± 9.2 ms in the DNA-bound form. Figure 3d shows the ^{1}H-^{15}N steady-state NOE of R2R3 in its DNA-bound and unbound forms. The averages of the NOE values for the R2 and R3 helical regions are 0.743 ± 0.120 and 0.735 ± 0.031 in the free form, and 0.742 ± 0.101 and 0.750 ± 0.073 in the DNA-bound form. In the free form the N-terminal four residues, Leu 90–Gly 93, show small NOE values, however, upon binding to DNA the NOE values of Ile 91, Lys 92, and Gly 93 become a little larger. Six residues in the connecting loop of R2 and R3, Glu 141–Ser 146, show larger NOE values in the DNA-bound form compared to the corresponding NOE values in the free form. The C-terminal three amino acids, Arg 191–Val 193, exhibit small NOE values in both the DNA-bound and unbound forms.

Figure 4a shows the T_1/T_2 values of R2R3 in the DNA-bound and unbound forms. The averages of the T_1/T_2 values of the R2 and R3 helical regions are 8.84 ± 2.41 and 6.62 ± 0.69 in the free form, and 14.3 ± 2.4 and 14.1 ± 2.4 in the DNA-bound form. The T_1/T_2 values of the N-terminal four residues, Leu 90–Gly 93, and the C-terminal five residues, Met 189–Val 193, are smaller than those of the other regions in both the free and DNA-bound forms. Large T_1/T_2 values were found for Trp 95, Thr 96, and Val 103 of R2, and Asp 178, Asn 179, Lys 182, Trp 185, Asn 186, and Thr 188 of R3 in the DNA-bound form. Figure 4b shows the $T_{1\rho}/T_2$ values. The averages of the $T_{1\rho}/T_2$ values of the R2 and R3 helical regions are 1.15 ± 0.18 and 1.00 ± 0.07 in the free form, and 1.21 ± 0.14 and 1.12 ± 0.10 in the DNA-bound form. In the free form the $T_{1\rho}$ value of each R3 residue is nearly equal to the T_2 value of the corresponding residue, however, the $T_{1\rho}$ value of each R2 residue is larger than the T_2 value of the corresponding residue. This indicates that conformational fluctuations on the micro- to milli-second time scale occur greatly in the R2 free form but not in the R3 free form. In the complex the $T_{1\rho}$ value of each of the R2 and R3 residues is larger than the T_2 value of the corresponding residue, suggesting that both R2 and R3 have chemical exchange contributions.

Model-Free Analysis—To evaluate the dynamical character of R2R3 in its DNA-bound form, here we assumed the isotropic motion of the 13 bp DNA complex of R2R3, and the relaxation data were analyzed by Lipari-Szabo model free analysis (*27, 28*) as modified by Clore *et al.* (*29, 30*). On comparison of the T_2 and $T_{1\rho}$ values of each amino acid in

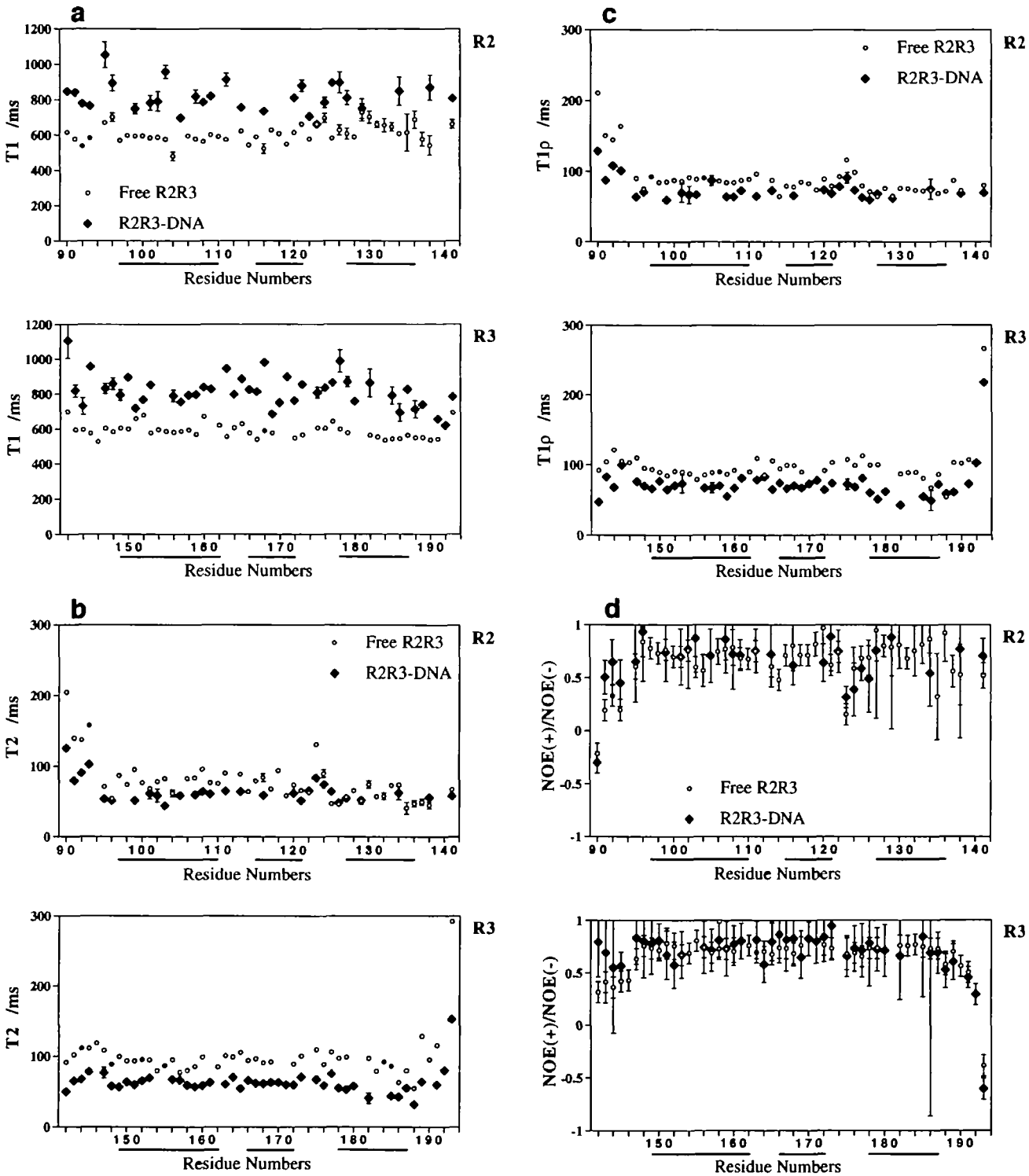

Fig. 3. **Plots of amide ^{15}N T_1, T_2, and $T_{1\rho}$, and ^1H-^{15}N steady-state NOE against the residue number.** (a) Longitudinal relaxation times, T_1. (b) Transverse relaxation times, T_2. (c) Longitudinal relaxation times in the rotating frame, $T_{1\rho}$. (d) Heteronuclear ^1H-^{15}N steady-state NOE values defined as $I_{NOE(+)}/I_{NOE(-)}$, where $I_{NOE(+)}$ and $I_{NOE(-)}$ are the integrated values of cross peaks with and without ^1H saturation, respectively. The error bars represent the uncertainties of the data. In the case of small uncertainties the error bars are hidden in the plots of the experimental values. The bars below the residue numbers indicate the helical regions.

the complex, the T_2 values of most amino acids of R2 and R3 seemed to contain severe chemical exchange contributions. Therefore to obtain the overall rotational correlation time (τ_R) we used the $T_1/T_{1\rho}$ values (shown in Fig. 4c) instead of the T_1/T_2 values, which are commonly used in the model free analysis. The overall rotational correlation time (τ_R) was calculated using the $T_1/T_{1\rho}$ values within the average $T_1/T_{1\rho}$ value ± 1SD for the residues having NOE values

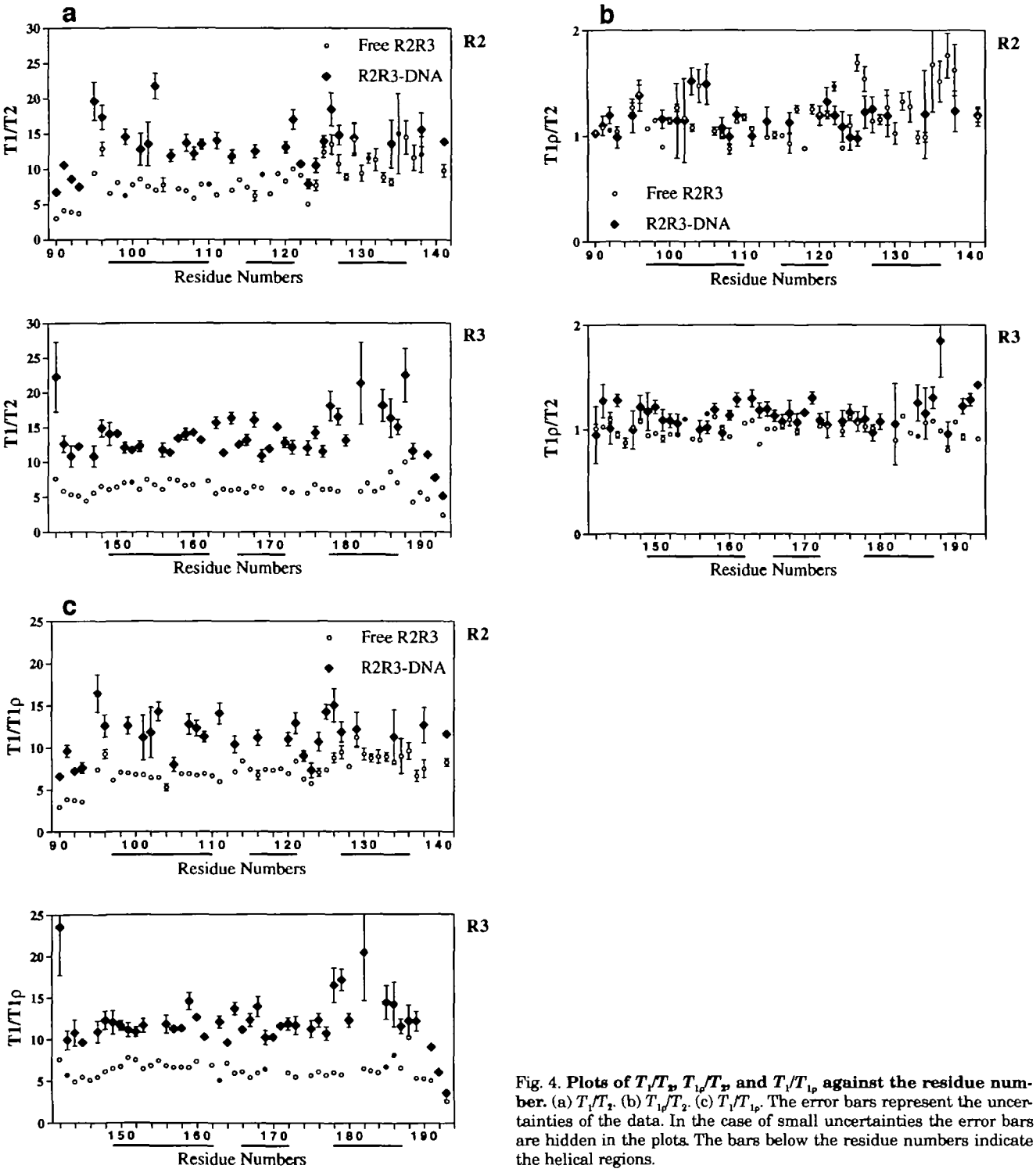

Fig. 4. **Plots of T_1/T_2, $T_{1\rho}/T_2$, and $T_1/T_{1\rho}$ against the residue number.** (a) T_1/T_2. (b) $T_{1\rho}/T_2$. (c) $T_1/T_{1\rho}$. The error bars represent the uncertainties of the data. In the case of small uncertainties the error bars are hidden in the plots. The bars below the residue numbers indicate the helical regions.

of above 0.7 in the helical regions. The calculated τ_R of R2R3 in the complex is 12.6 ± 0.05 ns, which is consistent for this size of molecule. T_1, T_2, and $T_{1\rho}$, ^1H-^{15}N steady-state NOE, and τ_R values were used in the model free analysis to obtain the generalized order parameter (S^2), the effective correlation time (τ_e), and the chemical exchange contribution (Rex) for each residue.

The calculated S^2 values are shown in Fig. 5a. The average S^2 values of the R2 and R3 helical regions are 0.831 ± 0.064 and 0.862 ± 0.049 in the free form, and 0.864 ± 0.069 and 0.851 ± 0.069 in the complex. In the free form of R2R3 the N-terminal four residues (Leu 90–Gly 93), the central three amino acids in the connecting loop between R2 and R3 (Glu 141, Lys 143, and Lys 144), and the C-terminal three residues (Met 189, Arg 191, and Val 193) exhibit smaller S^2 values as well as smaller NOE values,

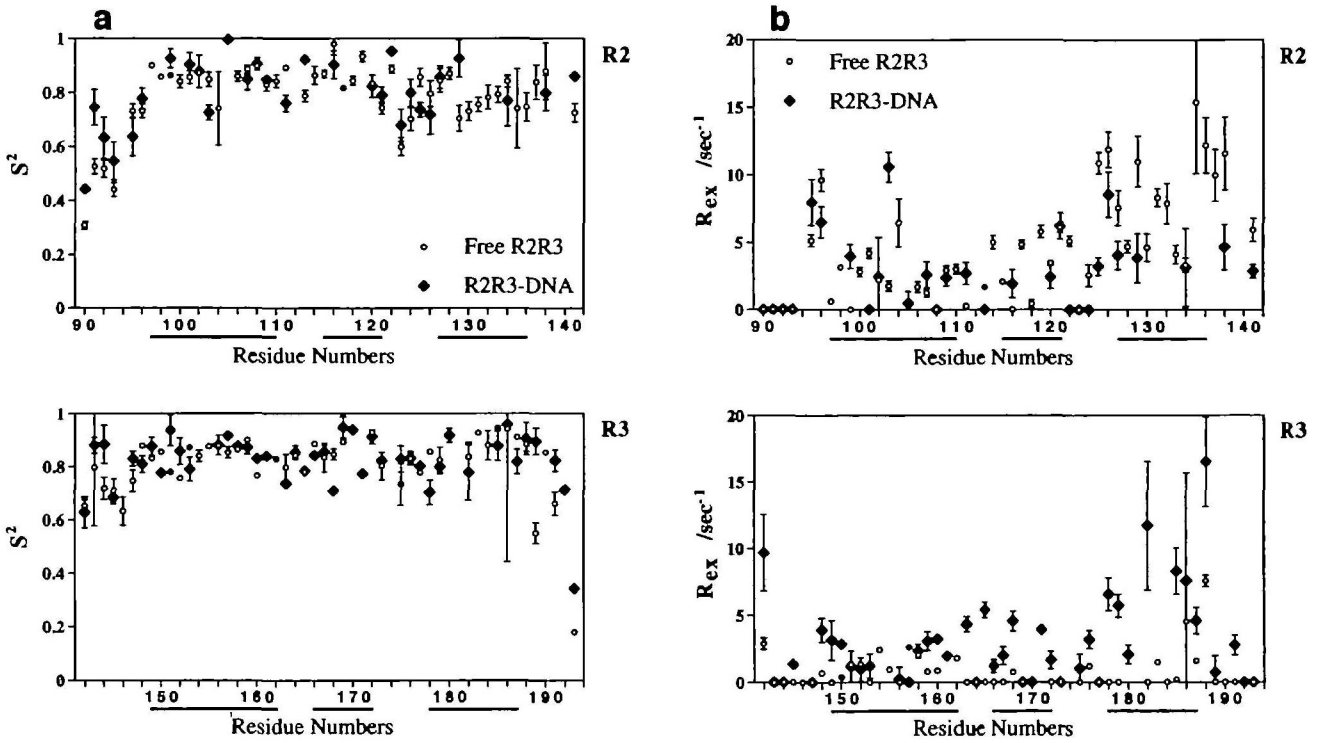

Fig. 5. **Plots of the generalized order parameters, S^2, and the chemical exchange parameters, Rex, against the residue number.** (a) The generalized order parameters, S^2. (b) The chemical exchange parameters, Rex. The error bars represent the uncertainties estimated from the covariance matrix of the optimized two or three parameter fits. In the case of small uncertainties the error bars are hidden in the plots of the calculated values. The bars below the residue numbers indicate the helical regions.

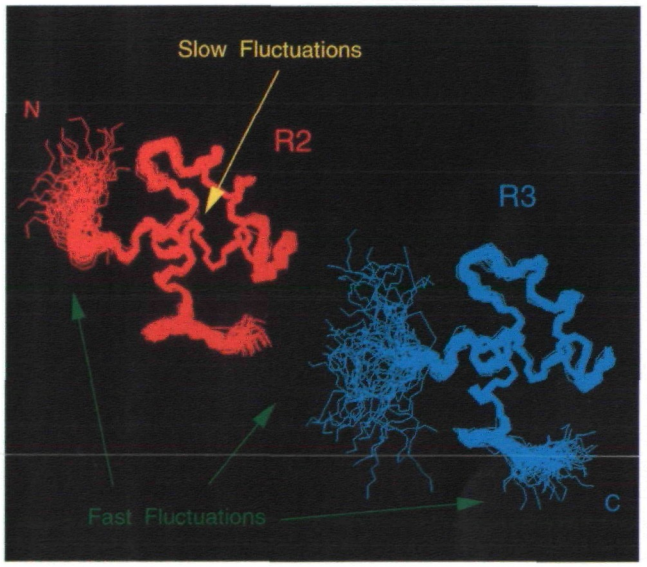

Fig. 6. **Mapping of the region exhibiting fast- and slow-fluctuations in free R2R3.** Superpositioning of the backbone atoms of 50 NMR structures in the R2 region is shown in red, and that in the R3 region in cyan.

indicating rapid motions of the backbones of these regions. Upon binding to DNA, the N-terminal four residues and the central three residues in the connecting loop, and the C-terminal three residues show larger NOE and S^2 values compared to those in the free form.

The calculated Rex values (shown in Fig. 5b) of Trp 95, Thr 96, and Val 103 in R2 are larger than 6.50. In the free form, the residues around the third helical region of R2, Ile 126, Gly 127, Gln 129, and Leu 138, showed large Rex values, while upon binding to DNA the Rex values of these amino acids were suppressed. In the complex the residues around the third helical region of R3, Asp 178, Asn 179, Lys 182, Trp 185, Asn 186, and Thr 188, exhibited large Rex values of more than 5.00.

DISCUSSION

Fast Motion—In the free form the N-terminal four residues (Leu 90–Gly 93), the central six residues in the connecting loop between R2 and R3 (Glu 141–Ser 146), and the C-terminal two residues (Arg 191 and Val 193) showed rapid motions on the pico- to nano-second time scale with smaller NOE and S^2 values. Based on the NMR structure of R2R3, these regions do not form a rigid structure, and the two globular units of R2 and R3 are likely to be linked by a flexible loop consisting of the central six amino acids, Glu 141–Ser 146, as shown in Fig. 6 (*15*). On the other hand, upon binding to DNA the NOE and S^2 values of the N-terminal three residues, Ile 91–Gly 93, and the central three residues, Glu 141–Lys 143, in the connecting loop increase. In the complex these regions become moderately fixed through the interactions of Lys 92, Lys 144, and Ser 146 with the phosphate backbone of DNA, as shown in Fig. 7 (*32–37*), which is consistent with the earlier observations for the DNA binding of topoisomerase I, Lac repressor, ADR1, and TFIIIA. In these cases a connecting loop or turn

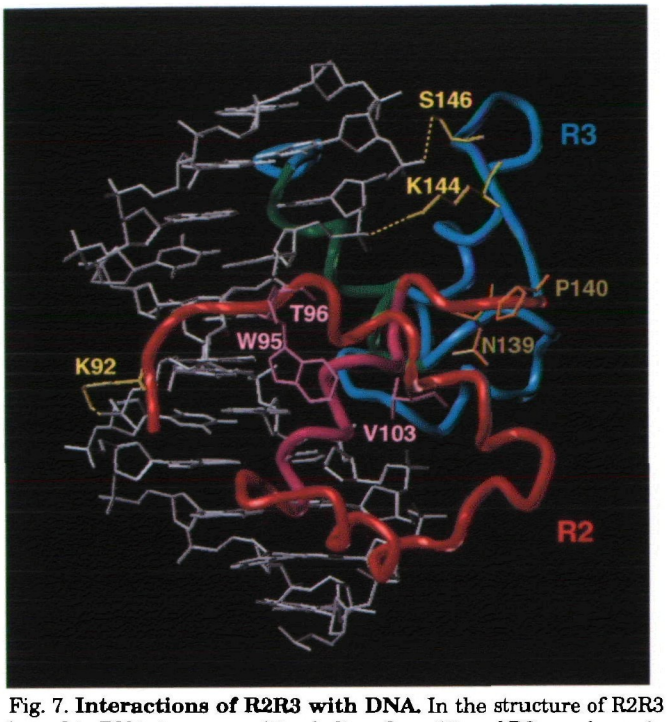

Fig. 7. **Interactions of R2R3 with DNA.** In the structure of R2R3 bound to DNA, two recognition helices from R2 and R3 are shown in magenta and green, the remaining parts of R2 and R3 being shown in red and cyan, respectively. Double-stranded DNA is shown as white lines. The side-chains of Trp 95, Thr 96, and Val 103 are shown in pink, and those of Asn 139 and Pro 140 in orange. The side-chains of Lys 92 in the N-terminus, and Lys 144 and Ser 146 in the repeat connecting loop are shown in yellow, and the contacts of these sidechains with DNA are shown as yellow dots.

between the rigid secondary structures becomes less flexible upon binding to DNA (*32–35*). The results of systematic mutation analysis of the DNA-binding domain of c-Myb suggested that a unique conformation around Asn 139 and Pro 140 of the loop in the complex (shown in Fig. 7) is important for the specific DNA-binding (*36, 37*).

Chemical Exchange Contributions—The chemical exchange contributions have been observed in R2 in the unbound form, especially in the third helical region. These chemical exchange contributions are caused by a cavity in the hydrophobic core of R2. For the cavity-filled mutant, in which Val 103 is replaced by a leucine residue, the chemical exchange contributions of R2 are greatly suppressed. Because the cavity-filled mutant has weaker DNA-binding activity than the wild type, the cavity of R2 was proposed to be important for a conformational change of R2 upon specific binding to DNA. In fact, for the DNA complex of R2R3 it has been shown that Trp 95 moves into the cavity to fill it up (*17*). In the complex, since the chemical exchange contributions between protein and DNA moieties should be taken into account (*38–40*), we need to be careful when evaluating the chemical exchange contributions of R2. However, the chemical exchange contributions of R2 are certainly suppressed in the complex compared to in the free form, except in the cases of amino acids Glu 99, Val 103, and Ser 116, as judged from the $T_{1\rho}/T_2$ and Rex values. In particular, amino acids around the third helix of R2, Arg 125, Ile 126, Gln 129, and Leu 138, exhibit much smaller chemical exchange contributions in the complex than in the free form. This is well correlated with the fact that R2 in the complex becomes thermally stable with a T_m of 58°C, at which the three repeats-DNA complex simultaneously melts, in contrast to the unstable property of R2 compared to the stable R1 and R3 in the free form (*16*). The suppression of the chemical exchange contributions of R2 in the complex is likely to be caused by the interaction of R2 with the phosphate backbone of DNA and by the conformational change of R2 upon binding to DNA.

It is interesting to note that in the complex Trp 95, Thr 96, and Val 103 still exhibit significant exchange contributions. In the complex Trp 95 moves into the cavity surrounded by Val 103, Cys 130, and Arg 133. Although the dynamics of Cys 130 and Arg 133 could not be obtained due to severe overlapping, even in the complex the altered R2 structure is likely to still be fluctuating on a micro- to millisecond time scale. Upon binding to DNA, the chemical shift changes of ^{15}N and ^{1}H signals of Thr 96 are the greatest, probably due to the conformational change of Trp 95, that has a strong ring current effect. Therefore, even a slight reorientation of Trp 95 can significantly affect the line width of the signal from the neighboring NH group in the complex (*17*).

As described, the overall chemical exchange contributions of the R2 moiety are suppressed in the complex compared to in the free form. However, the complex still exhibit significant chemical exchange contributions. In the free form the R3 moiety showed no significant chemical exchange contributions, however, upon binding to DNA, significant exchange contributions are observed in the R3 moiety, especially around the third helical region of R3. Although most of the signals of amino acids around the third helical region of R2 could not be analyzed because of signal overlaps and signal broadening effects of these amino acids, the third helical regions of both R2 and R3 are considered to have similar chemical exchange contributions. In the complex both third helices are located in the major groove of DNA and recognize a specific base sequence in a cooperative manner. Our present results suggest that the surface interaction between R2R3 and DNA might be changing on a micro- to milli-second time scale. In this study we measured both T_2 and $T_{1\rho}$. In the case of $T_{1\rho}$ measurements, since we used a spin lock power of 2.1 kHz, the chemical exchange contribution slower than a few hundred microseconds could be eliminated in $T_{1\rho}$ values. However, a little larger $T_1/T_{1\rho}$ values are observed for Trp 95 and amino acids in the third helical region of R3, Asp 178, Asn 179, and Lys 182, compared to in other regions. This suggests that these amino acids are being chemically exchanged on a time scale faster than a few hundred microseconds, in addition to the millisecond motions.

REFERENCES

1. Graf, T. (1992) Myb: A transcriptional activator linking proliferation and differentiation in hematopoietic cells. *Curr. Opin. Gen. Dev.* **2**, 249–255
2. Ness, S.A. (1996) The Myb oncoprotein: regulating a regulator. *Biochim. Biophys. Acta* **1288**, F123–139
3. Lipsick, J.S. (1996) One billion years of Myb. *Oncogene* **13**, 223–235
4. Oh, I-H. and Reddy, E.P. (1999) The *myb* gene family in cell growth, differentiation and apoptosis. *Oncogene* **18**, 3017–3033
5. Biedenkapp, H., Borgmeyer, U., Sippel, A.E., and Klempnauer,

K.-H. (1988) Viral *myb* oncogene encodes a sequence-specific DNA-binding activity. *Nature* **335**, 835–837
6. Weston, K. (1992) Extension of the DNA binding consensus of the chicken c-Myb and v-Myb proteins. *Nucleic Acids Res.* **20**, 3043–3049
7. Tanakawa, J., Yasukawa, T., Enari, M., Ogata, K., Nishimura, Y., Ishii, S., and Sarai, A. (1993) Recognition of specific DNA sequence by the c-myb proto-oncogene product: Role of three repeat units in the DNA-binding domain. *Proc. Natl. Acad. Sci. USA* **90**, 9320–9324
8. Oda, M., Furukawa, K., Ogata, K., Sarai, A., Ishii, S., Nishimura, Y., and Nakamura, H. (1997) Investigation of the pyrimidine preference by the c-Myb DNA-binding domain at the initial base of the consensus sequence. *J. Biol. Chem.* **272**, 17966–17971
9. Mücenski, M.L., McLain, K., Kier, A.B., Swerdlow, S.H., Schereiner, C.M., Miller, T.A., Pietryga, D.W., Scott, W.J., and Potter, S.S. (1991) A functional *c-myb* gene is required for normal murine fetal hepatic hematopoiesis. *Cell* **65**, 677–689
10. Sakura, H., Kanei-Ishii, C., Nagase, T., Nakagashi, H., Gonda, T.J., and Ishii, S. (1989) Delineation of three functional domains of the transcriptional activator encoded by the *c-myb* protooncogene. *Proc. Natl. Acad. Sci. USA* **86**, 5758–5762
11. Gonda, T.J., Gough, N.M., Dunn, A.R., and de Blaquiere, J. (1985) Nucleotide sequence of cDNA clones of the murine *myb* protooncogene. *EMBO J.* **4**, 2003–2008
12. Klempnauer, K.-H. and Sippel, A.E. (1987) The highly conserved amino-terminal region of the protein encoded by the *v-myb* oncogene functions as a DNA-binding domain. *EMBO J.* **6**, 2719–2725
13. Kanei-Ishii, C., Sarai, A., Sawazaki, T., Nakagoshi, H., He, D.-N., Ogata, K., Nishimura, Y., and Ishii, S. (1990) The tryptophan cluster: a hypothetical structure of the DNA-binding domain of the *myb* protooncogene product. *J. Biol. Chem.* **265**, 19990–19995
14. Ogata, K., Hojo, H., Aimoto, S., Nakai, T., Nakamura, H., Sarai, A., Ishii, S., and Nishimura, Y. (1992) Solution structure of a DNA-binding unit of Myb: a helix-turn-helix-related motif with conserved tryptophans forming a hydrophobic core. *Proc. Natl. Acad. Sci. USA* **89**, 6428–6432
15. Ogata, K., Morikawa, S., Nakamura, H., Hojo, H., Yoshimura, S., Zhang, R., Aimoto, S., Ametani, Y., Hirata, Z., Sarai, A., Ishii, S., and Nishimura, Y. (1995) Comparison of the free and DNA-complexed forms of DNA-binding domain from c-Myb. *Nat. Struct. Biol.* **2**, 309–320
16. Sarai, A., Uedaira, H., Morii, H., Yasukawa, T., Ogata, K., Nishimura, Y., and Ishii, S. (1993) Thermal stability of the DNA-binding domain of the Myb oncoprotein. *Biochemistry* **32**, 7759–7764
17. Ogata, K., Kanei-Ishii, C., Sasaki, M., Hatanaka, H., Nagadoi, A., Enari, M., Nakamura, H., Nishimura, Y., Ishii, S., and Sarai, A. (1996) The cavity in the hydrophobic core of Myb DNA-binding domain is reserved for DNA recognition and trans-activation. *Nat. Struct. Biol.* **3**, 178–187
18. Ogata, K., Morikawa, S., Nakamura, H., Sekikawa, A., Inoue, T., Kanai, H., Sarai, A., Ishii, S., and Nishimura, Y. (1994) Solution structure of a specific DNA complex of the Myb DNA-binding domain with cooperative recognition hericies. *Cell* **79**, 639–648
19. Messerle, B.A., Wider, G., Otting, G., Weber, C., and Wüthrich, K. (1989) Solvent suppression using a spin lock in 2D and 3D NMR spectroscopy with H_2O solution. *J. Magn. Reson.* **85**, 608–613
20. Kay, L.E., Marion, D., and Bax, A. (1989) Practical aspects of 3D heteronuclear NMR of protein. *J. Magn. Reson.* **84**, 7284
21. Marion, D., Driscoll, P.C., Kay, L.E., Wingfield, P.T., Bax, A., Gronenborn, A.M., and Clore, G.M. (1989) Overcoming the overlap problem in the assignment of ^1H NMR spectra of large proteins by use of three-dimensional heteronuclear ^1H-^{15}N Hartman-Hahn multiple quantum coherence spectroscopy: application to interleukin 1b. *Biochemistry* **28**, 6150–6156
22. Kay, L.E., Torchia, D.A., and Bax, A. (1989) Backbone dynamics of proteins as studied by ^{15}N inverse detected heteronuclear NMR spectroscopy: application to staphylococcal nuclease. *Biochemistry* **28**, 8972–8979
23. Kay, L.E., Nicholson, L.K., Delaglio, F., Bax, A., and Torchia, D.A. (1992) Pulse sequence for removal of the effects of cross correlation between dipolar and chemical-shift anisotoropy relaxation mechanisms on the measurement of heteronuclear T_1 and T_2 values in proteins. *J. Magn. Reson.* **97**, 359–375
24. Peng, J.W., Thanabal, V., and Wagner, G. (1991) 2D heteronuclear NMR measurements of spin-lattice relaxation times in the rotating frame of X nuclei in heteronuclear HX spin system. *J. Magn. Reson.* **94**, 82–100
25. Szyperski, T., Luginbuhl, P., Otting, G., Guntert, P., and Wüthrich, K. (1993) Protein dynamics studied by rotating frame ^{15}N spin relaxation times. *J. Biomol. NMR* **3**, 151–164
26. Press, W.H., Flannery, B.P., Teukolsky, S.A., and Vetterling, W.T. (1993) *Numerical Recipes in FORTRAN* 2nd ed., Cambridge University Press, Cambridge
27. Lipari, G. and Szabo, A. (1982) Model-free approach to the interpretation of nuclear magnetic resonance relaxation in macromolecules. 1. Theory and range of validity. *J. Am. Chem. Soc.* **104**, 4546–4559
28. Lipari, G. and Szabo, A. (1982) A model-free approach to the interpretation of nuclear magnetic resonance relaxation in macromolecules. 2. Analysis of experimental results. *J. Am. Chem. Soc.* **104**, 4559–4570
29. Clore, G.M., Szabo, A., Bax, A., Kay, L.E., Driscoll, P.C., and Gronenbon, A.M. (1990) Deviations from the simple two-parameter model-free approach to the interpretation of nitrogen-15 nuclear magnetic relaxation in proteins. *J. Am. Chem. Soc.* **112**, 4989–4991
30. Clore, G.M., Driscoll, P.C., Wingfield, P.T., and Gronenbon, A.M. (1990) Analysis of the backbone dynamics of interleukin-1β using two-dimensional inverse detected heteronuclear ^{15}N-^1H NMR spectroscopy. *Biochemistry* **29**, 7387–7401
31. Constantin, K.L., Friedrichs, M.S., Goldfarb, V., Jeffrey, P.D., Sheriff, S., and Mueller, L. (1993) Characterization of the backbone dynamics of an anti-digoxin antibody VL domain by inverse detected ^1H-^{15}N NMR: Comparisons with X-ray data for the Fab. *Proteins* **15**, 290–311
32. Yu, L., Zhu, C.X., Tse-Dinh, Y.C., and Fesik, S.W. (1996) Backbone dynamics of the C-terminal domain of *Escherichia coli* topoisómerase I in the absence and presence of single-stranded DNA. *Biochemistry* **35**, 9661–9666
33. Slijper, M., Boelens, R., Davis, A.L., Konings, R.N.H., van der Marel, G.A., van Boom, J.H., and Kaptein, R. (1997) Backbone and side chain dynamics of lac repressor headpiece (1–56) and its complex with DNA. *Biochemistry* **36**, 249–254
34. Hyre, D.E. and Klevit, R.E. (1998) A disorder-to-order transition coupled to DNA binding in the essential zinc-finger DNA-binding domain of yeast ADR1. *J. Mol. Biol.* **279**, 929–943
35. Foster, M.P., Wuttke, D.S., Radhakrishnan, I., Case, D.A., Gottesfeld, J.M., and Wright, P.E. (1997) Domain packing and dynamics in the DNA complex of the N-terminal zinc fingers of TFIIIA. *Nat. Struct. Biol.* **4**, 605–608
36. Oda, M., Furukawa, K., Ogata, K., Sarai, A., and Nakamura, H. (1992) Thermodynamics of specific and non-specific DNA binding by the c-Myb DNA-binding domain. *J. Mol. Biol.* **276**, 571–590
37. Oda, M., Furukawa, K., Sarai, A., and Nakamura, H. (1999) Kinetic analysis of DNA binding by the c-Myb DNA-binding domain using surface plasmon resonance. *FEBS Lett.* **454**, 288–292
38. Spolar, R. and Record, T., Jr. (1994) Coupling of local folding to site-specific binding of protein to DNA. *Science* **263**, 777–784
39. Jin, C., Marsden, J., Chen, X., and Liao, X. (1999) Dynamic DNA contacts observed in the NMR structure of winged helix protein-DNA complex. *J. Mol. Biol.* **289**, 683–690
40. Jin, C. and Liao, X. (1999) Backbone dynamics of a winged helix protein and its DNA complex at different temperatures: changes of internal motions in Genesis upon binding to DNA. *J. Mol. Biol.* **292**, 641–651